Available on the CERN CDS information server

CMS PAS FSQ-14-001
TOTEM-NOTE-2014-002

CMS–TOTEM Physics Analysis Summary

Contact: cms-pag-conveners-fsq@cern.ch

2014/10/13

CMS-TOTEM feasibility studies for single diffractive Z, W, J/ψ and central exclusive dijet production in pp collisions at $\sqrt{s} = 13$ TeV

The CMS and TOTEM Collaborations

Abstract

Feasibility studies for the measurement of single-diffractive Z or W boson production in the electron and muon channels, J/ψ production in the muon decay channel and central exclusive dijet production, in proton-proton (pp) collisions with the Compact Muon Solenoid (CMS) and TOTal Elastic and diffractive cross section Measurement (TOTEM) experiments are presented. Visible cross sections are defined for such processes and presented along with the expected event yields based on the Large Hadron Collider (LHC) Run II high-β^* beam optics configuration, low-pileup scenario, assuming an integrated luminosity of 10 pb^{-1}.

1 Introduction

In this study, the *visible* cross sections and event yields is estimated, based on the Monte Carlo (MC) simulation of the CMS detector, for single-diffraction (SD) and central exclusive dijet production (CEP). Figure 1 shows a sketch for SD production, pp $\rightarrow$ Xp, where the system X includes a Z or W boson, or J/ψ meson, and for CEP, pp $\rightarrow$ pJJp, where JJ is a dijet system. In diffractive events the energy of the outgoing proton(s) or corresponding low-mass state is approximately such for the incoming proton(s). These interactions proceed by a color-singlet exchange and the two groups of final-state particles are well separated with a large gap in rapidity, a "large rapidity gap" (LRG) [1, 2]. Diffractive hadron-hadron scattering can be described within Regge theory [3, 4]. In this framework diffraction is characterized by the exchange of the pomeron ($\mathbb{P}$) [5] trajectory, which has the vacuum quantum numbers, and hence no color. The single-diffractive production is sensitive to the diffractive structure function of the proton, notable its quark component, since many of the observed diffractive masses can originate from quark fusion (Z or W boson and J/ψ production). In addition, CEP processes explores gluon fusion component and have a clean topology that can be used to supress many physics backgrounds for new physics searches [6, 7].

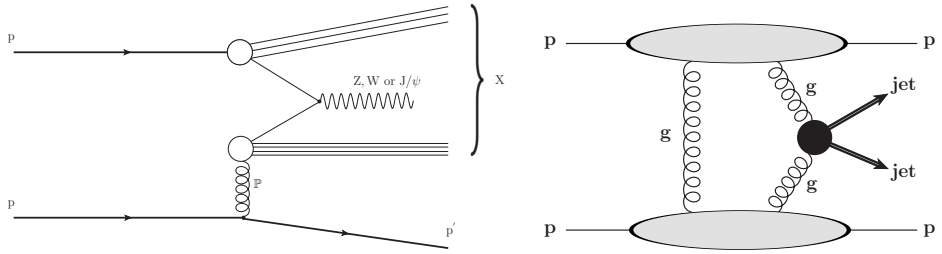

Figure 1: Single diffractive Z, W and J/ψ production (left) and central exclusive dijet production (right).

Two experimental signatures can therefore be used to study diffractive processes: the presence of a LRG in the final state, or the measurement of a very energetic forward outgoing proton. In high-mass diffractive production at the LHC, the position of the LRG is mostly outside the acceptance of the CMS detector (Ref. [8]). On the other hand, Roman pot (RP) detectors from the TOTEM experiment can accurately measure the outgoing proton properties. The present study exploits RP detectors to identify diffractive processes by measuring the outgoing protons.

The expected event yields is presented for low-luminosity, low-pileup running at the LHC, for a range of processes which illustrate the potential for physics measurements with the CMS and TOTEM experiments at the beginning of Run II. The results shown are not meant as full feasibility studies but rather estimates of the expected signal contribution and of the detector acceptance. As such, the different sources of physics and beam backgrounds, as well as the effect of the trigger selection and systematic uncertainties are not covered in detail but are briefly discussed in Section 5.

In the following, the visible cross section (σ_{vis}) is taken as the simulated cross section corrected by the effect of selection cuts at detector level. It is defined as:

$$\sigma_{\text{vis}} = \frac{\text{N}_{\text{sel}}}{\text{N}_{\text{tot}}}\sigma_{\text{mc}} \tag{1}$$

where σ_{mc} is the Monte Carlo cross section for each process, N_{sel} the number of events selected and N_{tot} the total number of Monte Carlo events.

1.1 LHC Run II low-pileup scenarios

Two LHC beam optics scenarios (Table 1) have been assumed both with low-pileup and high-$\beta^* = 90$ m, which is the betatron amplitude function at the interaction point (IP). A high value of β^* corresponds to large beam size and small angular spread.

Table 1: Overview of the expected running scenarios. The ranges of the average number of inelastic pileup interactions and the delivered luminosity are shown in the two right-most columns. The precise values depend on the number of protons in a bunch (N), the number of bunches (k), and the emittance ϵ_N.

β^* [m]	crossing angle [μrad]	ϵ_N [μm rad]	N [10^{11}]	k [bunches]	μ	Luminosity [pb^{-1}/24h]
90	0	2	[0.5 - 1.5]	156	[0.06 - 0.5]	[0.1 - 1]
90	100	2	[0.5 - 1.5]	1000	[0.06 - 0.5]	[0.8 - 7]

Assuming high-β^* running, two weeks of CMS and TOTEM common data taking would mean:

- an integrated luminosity of 10 pb^{-1} which can be obtained with a large number of bunches (k), crossing angle and $\mu \sim 0.1$ or with few bunches (k), no crossing angle and $\mu \sim 0.5$. This last scenario has been choosen to be used in this analysis.
- an integrated luminosity of 100 pb^{-1} with a large number of bunches (k), crossing angle and $\mu \sim 0.5$. A detailed description can be found in Ref. [9, 10].

2 Experimental setup

2.1 CMS detector

The CMS apparatus features a superconducting solenoid, 12.5 m long with an internal diameter of 6 m, providing a uniform magnetic field of 3.8 T. Within the field volume are a silicon pixel and strip tracker, a crystal electromagnetic and a brass/scintillator hadron calorimeter. The momentum resolution for reconstructed tracks in the central region is about 1.5% for non-isolated particles with transverse momenta (p_T) between 1 and 10 GeV and 2.8% for isolated particles with p_T of 100 GeV. The calorimeter system surrounds the tracker and consists of a scintillating lead-tungstate crystal electromagnetic and a brass/scintillator hadron calorimeter with coverage up to $|\eta|$=3. The quartz/steel forward hadron calorimeters extend the calorimetry coverage up to $|\eta|$=5.

The very forward angles are instrumented at one end of CMS ($-6.6 < \eta < -5.2$) by the CASTOR calorimeter [11]. CASTOR is made of quartz fibers/plates embedded in tungsten absorbers, segmented in 16 ϕ-sectors and 14 $z-$modules. Forward Shower Counter (FSC) detectors [12] are located on both sides of the IP. They are a set of 10-12 scintillation counters designed to detect showers produced by particles hitting the beam pipes and surrounding material and cover the very forward pseudo-rapidity range $6 \lesssim |\eta| \lesssim 8$.

A system of gas-ionization muon detectors embedded in the steel flux-return yoke of the solenoid allows reconstruction and identification of muons in the $|\eta| < 2.4$ region. Events are recorded using a two-level trigger system. A more detailed description of the CMS detector and the trigger system can be found in [13].

Offline, particle candidates are individually identified using a particle-flow reconstruction [14, 15]. This algorithm reconstructs each particle produced in a collision by combining information from the tracker, the calorimeters, and the muon system, and identifies them as either a charged

hadron, neutral hadron, photon, muon, or electron. The candidate particles are then clustered into jets using the anti-k_T algorithm [16] with a distance parameter of 0.5. The energy resolution for jets is 15% at p_T of 10 GeV, 8% at p_T of 100 GeV, and 4% at p_T of 1 TeV [17]. Corrections are applied to the jet four-momenta as a function of the jet p_T and η to account for residual effects of non-uniform detector response [18]. The E_T^{miss} in this analysis is defined as the magnitude of the vector sum of the transverse momenta of all particles reconstructed in the event, excluding muons.

2.2 TOTEM Roman pot detectors

The TOTEM experiment [19, 20] is composed of three subdetectors: the T1, T2 telescopes and a series of RP stations on both sides of the IP. The T1 and T2 telescopes are placed symmetrically on each side of the IP at about $|z| = 11$ m and $|z| = 14$ m. Each tracker T1 is made up of 5 planes perpendicular to the beam line. In each T2 arm, 20 semi-circular GEM planes, with overlapping regions, are interleaved on both sides of the beam vacuum chamber to form ten detector planes with a full coverage.

Every RP station is composed of two units, separated by a distance of 4-10 m. Each unit consists of two pots in the vertical plane approaching the beam from above and below, and one that moves horizontally. They are placed very far from the IP (about $204 - 214$ and $215 - 220$ m), on both sides of the IP. Each RP is equipped with a telescope of 10 silicon microstrip sensors of 66 μm pitch which provides spatial track reconstruction resolution $\sigma(x, y)$ of 11 μm. Given the longitudinal distance between the units of $\Delta s = 4 - 10$ m the proton angles are measured by the RPs with an uncertainty of a few μrad.

3 Monte Carlo model

The fractional momentum loss of the outgoing proton, defined as $\xi = 1 - p'/p$, where p (p′) is the momentum of the incident (scattered) proton, and the four-momentum transfer squared defined as $t = (p - p')^2$, were used to characterize the event at generator level.

The simulation and reconstruction software used in this study do not include the description of both CMS and TOTEM Roman pot detectors. An acceptance table as a function of ξ and t has instead been used which quantifies the probability that a proton is measured in each RP detector station. The detailed Monte Carlo simulation of the CMS detector response is based on GEANT4 [21].

Events were simulated with overlapping pp interactions in the same bunch crossing (i.e. pileup). In the simulation, one main (signal) event is produced corresponding to a given physics process, as discussed below. Pileup events are added to the main event with probability $p(n; \mu)$, where n is the number of pileup events, given by a Poisson distribution with an average of $\mu = 1$. This value is considered as an upper limit in the expected running scenario of high-β^* beam optics configuration, characterized by low pileup ($\mu \ll 1$ or up to $\mu = 0.5$, see Section 1.1), assuming a more pessimistic than expected scenario. Pileup events were simulated using the PYTHIA8 Monte Carlo event generator [22]. They were simulated as inelastic, minimum-bias events, using the PYTHIA8 Tune A2. The outgoing protons from pileup events are not included in the simulation.

SD Z or W production is simulated with the POMWIG Monte Carlo event generator [23], version v2.0 beta, single-diffractive J/ψ production is simulated with POMPYT v2.6 [24] and CEP dijet production with EXHUME v1.3.3 [25].

3.1 SD Z or W boson production

Single-diffractive Z or W boson production was simulated with POMWIG, in the electron and muon decay channels; 50 000 events were simulated in each decay channel. POMWIG is a modified version of HERWIG [26], which can generate diffractive interactions while retaining all the standard HERWIG hard subprocesses for pomeron-proton, photon-pomeron and pomeron-pomeron collisions. The NLO H1 2006 fit B [27] is used for the diffractive parton density functions (dPDF) and the pomeron flux calculation. Specifically, for the parameterized flux factor the following values were used: $\alpha_{\mathbb{P}}(0) = 1.111$, $\alpha' = 0.06\ \mathrm{GeV}^{-2}$ and $\beta_{\mathbb{P}} = 5.5\ \mathrm{GeV}^{-2}$ [23]. For the inclusive proton PDF, the CTEQ6M [28] parameterization was used. Events were simulated in the kinematic range $\xi < 0.2$ and $|t| < 4\ \mathrm{GeV}^{-2}$.

In hadron-hadron collisions, the diffractive cross section is suppressed by the effect of soft rescattering among spectator partons, which fill the LRG. This suppression is often quantified by a "rapidity gap survival probability" ($\langle|S^2|\rangle$). The predictions presented in this study include a rapidity gap survival probability of $\langle|S^2|\rangle = 10\%$, which describes well the CMS diffractive dijet data [29]. According to POMWIG, the cross section, including the branching fraction $\mathcal{B}$ for the diffractive production of a Z boson ($\sigma_{\mathrm{mc,\,Z}} \times \mathcal{B}(Z \to ll)$) is 12.1 pb and for the diffractive production of a W boson ($\sigma_{\mathrm{mc,\,W}} \times \mathcal{B}(W \to l\nu)$) 131 pb.

3.2 SD J/ψ production

For single-diffractive J/ψ production, 100 000 events were simulated with POMPYT. The POMPYT Monte Carlo event generator is based on the Ingelman and Schlein approach [30], which considers the diffractive reaction as a two-step process: one proton exchanges a pomeron with fractional momentum ξ, which then interacts with the other proton. This generator was used with dPDFs from the results of the diffractive deep inelastic scattering data (H1 fit B [27]). For the inclusive proton PDF, the CTEQ6L1 parameterization was used. Events were generated with the PYTHIA6 D6T tune [31]. The parameterization of the pomeron flux in POMPYT is also based on the QCD fits to the HERA data. Events were generated in the kinematic range, $p > 2.5$ GeV, $|\eta| < 2.5$, $\xi < 0.2$, $|t| < 4\ \mathrm{GeV}^{-2}$, where p is the muon momentum and η its pseudorapidity. A gap survival probability of $\langle|S^2|\rangle = 10\%$ was used. The cross section for diffractive J/ψ ($\sigma_{\mathrm{mc,\,J/\psi}} \times \mathcal{B}(J/\psi \to \mu\mu)$) is 2.5 nb.

3.3 CEP dijet production

The EXHUME Monte Carlo event generator is based on the perturbative QCD calculation of Khoze, Martin and Ryskin [32] of the process pp $\to$ pXp, where X is a centrally produced color-singlet system. In such processes, there is no radiation other than that from the central system, and two outgoing protons. EXHUME uses the gluon fusion subprocess cross sections. For the central exclusive dijet channel, 50 000 events were simulated with a dijet system minimum invariant mass (M_{jj}^{Gen}) of 100 GeV and a survival probability of $\langle|S^2|\rangle = 10\%$. The cross section for central exclusive dijet production ($\sigma_{\mathrm{mc,\,CEP}}$) is 2.35 nb ($M_{jj}^{\mathrm{Gen}} > 100$ GeV).

In central exclusive processes, the parton densities are assumed to be the skewed unintegrated gluon densities of the proton. They depend on the transverse momentum exchanged as well as on the two longitudinal momentum fractions (x, x') carried by the exchanged gluons from a proton. In the region of interest ($x' \ll x \ll 1$) these densities can be approximated by the standard (integrated) gluon densities [33]. They each include a Sudakov factor, which gives the probability that the gluons do not radiate in their evolution from the initial scale (Q_T) up to the hard scale μ=M/2, where M is the mass of the central system. It is only relevant to the gluons initiating the hard subprocess.

4 Event selection

In this section the procedure used to select SD and CEP processes is presented. The estimates of the signal event yields take into account the acceptance of the RP detectors, which describes the probability that a proton is measured in the stations in either side of the interaction point. The Z or W boson, J/ψ meson and dijet final states are selected using the central CMS detector in the range $|\eta| < 2.5$.

4.1 RP detector acceptance

The acceptance is determined based on a parametrization of the proton propagation in the LHC beam line [34]. and defined as the probability that a proton is measured in a RP station, in bins of ξ and t. The protons are required to be within the fiducial region of the detectors inside the RPs. Figure 2 shows the simulated acceptance of a proton reaching the RP detector stations in either side of the IP, calculated using a distance of 5.6 mm between the edge of the silicon detectors in a RP and the beam position. The RP average acceptance for each direction, CMS z-negative (z-positive), is around 50%.

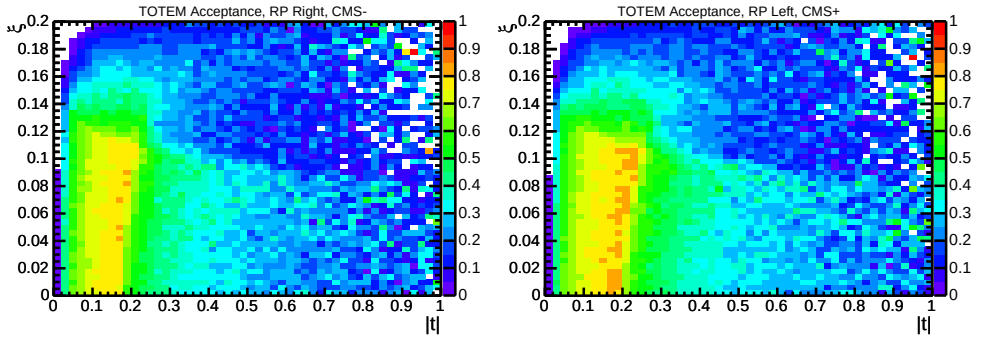

Figure 2: Acceptance of a proton detected in the RP stations in either the CMS z-negative (left) or z-positive (right) direction.

Figure 2 is compatible with the 8 TeV observed acceptance scaled to the expected beam configuration at 13 TeV [9]. The parametrization of the proton propagation along the LHC beam line has been validated using data taken simultaneously by CMS and TOTEM, in 2012, with similar conditions as those expected for the low-pileup scenarios during the LHC Run II in 2015 and $\beta^* = 90$ m.

4.2 Single-diffractive production

The following common preselection criteria were applied:

- A proton was required to be within the acceptance of the RP station in either side of the interaction point;
- A single reconstructed vertex was required. This cut rejects events with additional pileup interactions for which a primary vertex is reconstructed. Roughly 45% of events are selected by this cut, which depends directly on the conditions described in Section 3.

The Z or W selection follows that of [35]. The following criteria were used for $Z \to e^+e^-$ and $Z \to \mu^+\mu^-$:

- The two leading leptons (largest p_T) were required to have $p_T > 20$ GeV and to fulfill the isolation criteria described in [35] in order to avoid electrons from conver-

sion and to reject muon candidates reconstructed in QCD events. The isolation is calculated as a sum over the p_T of all tracks in a cone of radius 0.3 around the muon candidate. For electrons, ECAL and HCAL isolation criteria are also applied;

- The dilepton system invariant mass was required to be in the range $60 < M_{ll} < 110$ GeV.

For $W^{\pm} \to e^{\pm}\nu_e$ and $W^{\pm} \to \mu^{\pm}\nu_\mu$ the following criteria were applied:

- The leading lepton (largest p_T) was required to have $p_T > 20$ GeV and to fulfill the isolation criteria described above;
- Events with an additional lepton with $p_T > 10$ GeV are rejected;
- The transverse mass of the lepton-neutrino system was required to be in the range $60 < M_T < 110$ GeV. It was reconstructed as $M_T = \sqrt{2E_{T,l} \cdot E_{T,\nu}[1 - \cos(\phi_l - \phi_\nu)]}$. The missing transverse momentum (E_T^{miss}) is the transverse momentum imbalance of all the visible particles in the CMS detector and is used to estimate the transverse momentum and azimuthal direction of the neutrino candidate, $E_{T,\nu}$ and ϕ_ν.

For the $J/\psi \to \mu^+\mu^-$ selection, the following requirements were applied:

- At least two muons were required with opposite charge, with $|\eta| < 2.45$;
- In this analysis muon candidates are defined as tracks reconstructed in the silicon tracker, which are associated with a compatible signal in the muon chambers. For muon candidates, two approaches are considered: tracks are first reconstructed independently in the inner tracker (tracker track) and in the muon system (standalone-muon track). Based on these reconstructed tracks, for each standalone-muon track, a matching tracker track is found by comparing parameters of the two tracks propagated onto a common surface. A global-muon track is fitted combining hits from the tracker track and standalone-muon track, using the Kalman-filter technique; for the latter case, all tracker tracks with $p_T > 0.5$ GeV and total momentum $p > 2.5$ GeV are considered as possible muon candidates and are extrapolated to the muon system taking into account the magnetic field, the average expected energy losses, multiple Coulomb scattering in the detector material, and matched to locally reconstructed segments in muon detectors [36].
- The dimuon system invariant mass was required to be in the range $3.05 < M_{\mu^-\mu^+} < 3.15$ GeV.

Table 2 shows the overall fraction of events selected in each channel. A smaller fraction of selected events is observed when the proton is detected in the CMS negative z direction. However, for $Z \to e^+e^-$ selected events, this difference is negligible.

Table 2: Fraction of events selected in the $Z \to e^+e^-$, $Z \to \mu^+\mu^-$, $W \to e\nu_e$, $W \to \mu\nu_\mu$ and $J/\psi \to \mu^+\mu^-$ channels, shown for events with a proton detected in the CMS z-negative or z-positive direction.

	$Z \to e^+e^-$	$Z \to \mu^+\mu^-$	$W^+ \to e^+\nu_e$ $W^- \to e^-\bar{\nu}_e$	$W^+ \to \mu^+\nu_\mu$ $W^- \to \mu^-\bar{\nu}_\mu$	$J/\psi(\mu^+\mu^-)$
proton tagged on CMS z-positive or z-negative	0.111	0.169	0.125	0.155	0.133

Figure 3 shows the distributions of the pseudorapidity η and ξ of the protons tagged in the RP detector stations, in $Z \to e^+e^-$ events. Similar distributions for $Z \to \mu^+\mu^-$, $W^{\pm} \to e^{\pm}\nu_e$ and $W^{\pm} \to \mu^{\pm}\nu_\mu$ were observed. Figure 4 shows the distributions of t and ξ of protons tagged in

$J/\psi(\mu^+\mu^-)$ events.

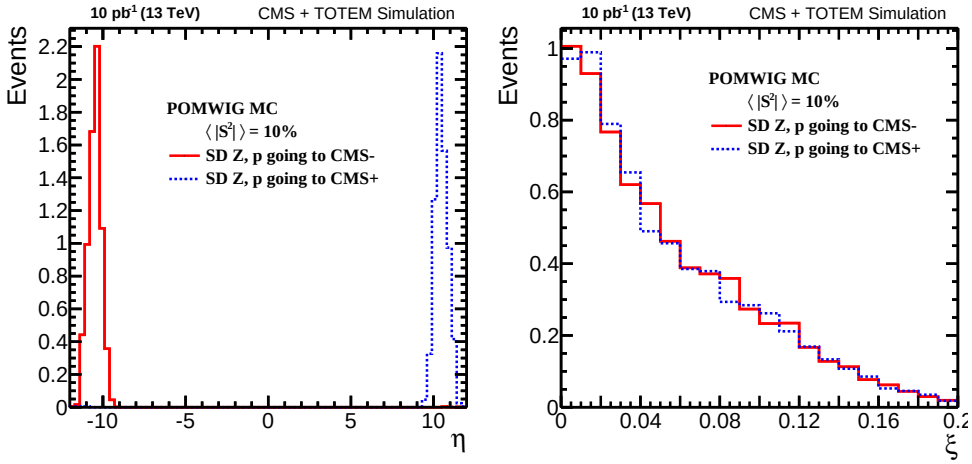

Figure 3: Distributions of the pseudorapidity η (left) and ξ (right) of the protons tagged in the RP detector stations in $Z \to e^+e^-$ events. Outgoing protons in the CMS z-negative direction are shown in red (solid line) and protons in the z-positive direction in blue (dashed line). Events were simulated with the POMWIG MC and normalized to an integrated luminosity of 10 pb^{-1}. A gap survival probability of 10% was used.

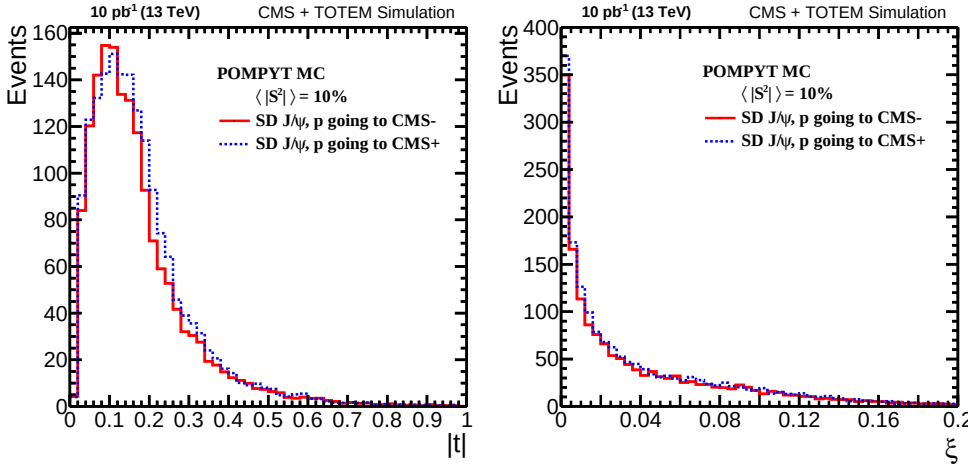

Figure 4: Distributions of t (left) and ξ (right) of protons tagged in the RP detector stations in $J/\psi(\mu^+\mu^-)$ events. Outgoing protons in the CMS z-negative direction are shown in red (solid line) and protons in the CMS z-positive direction in blue (dashed line). Events were simulated with the POMPYT MC and normalized to an integrated luminosity of 10 pb^{-1}. A gap survival probability of 10% was used.

Figure 5 shows distributions of the dilepton invariant mass of the leptons pseudorapidity in $Z \to e^+e^-$ events. They are similar in $Z \to \mu^+\mu^-$ events.

Figure 6 shows the distributions of the transverse mass and the leading lepton pseudorapidity in $W^\pm \to e^\pm\nu_e$ events.

Figure 7 shows the distributions of the pseudorapidity of the $J/\psi(\mu^+\mu^-)$ system and the transverse momentum of the leading muons in $J/\psi(\mu^+\mu^-)$ events.

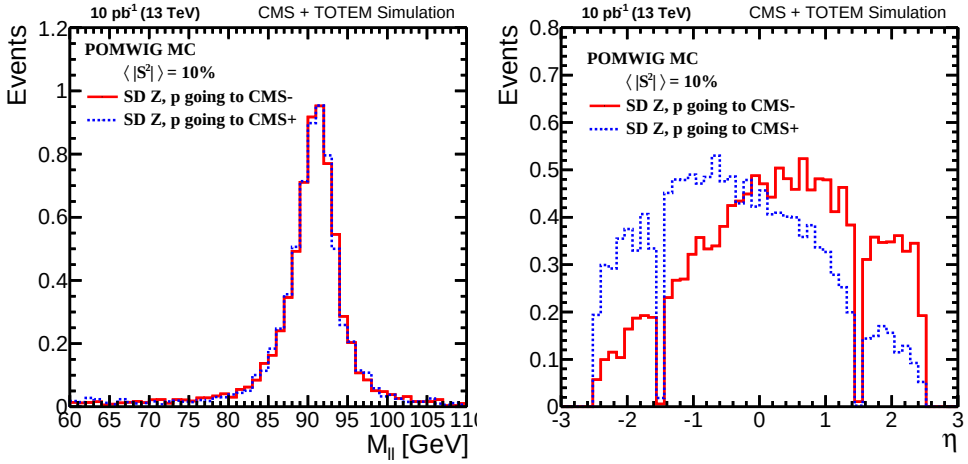

Figure 5: Distributions of the invariant mass (M_{ll}) of the dilepton system (left) and pseudorapidity of the leading leptons (right) for events with a proton tagged in the RP detector stations in $Z \to e^+e^-$ events. Events with a proton detected in the CMS z-negative (positive) direction are shown in solid red (dashed blue) line. Events were simulated with the POMWIG MC and normalized to an integrated luminosity of 10 pb^{-1}. A gap survival probability of 10% was used.

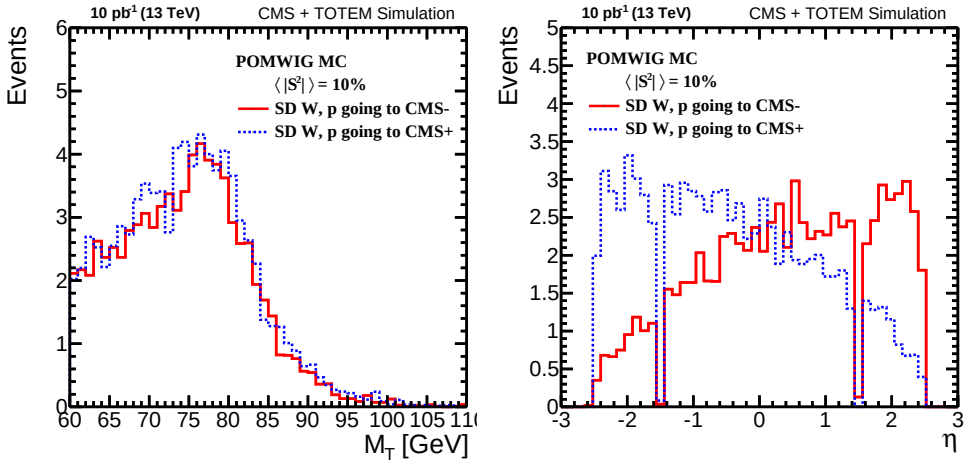

Figure 6: Distributions of the transverse mass M_T (left) and the leading lepton pseudorapidity (right) in $W^{\pm} \to e^{\pm}\nu_e$ events. Events with a proton detected in the CMS z-negative (positive) direction are shown in solid red (dashed blue) line. Events were simulated with the POMWIG MC and normalized to an integrated luminosity of 10 pb^{-1}. A gap survival probability of 10% was used.

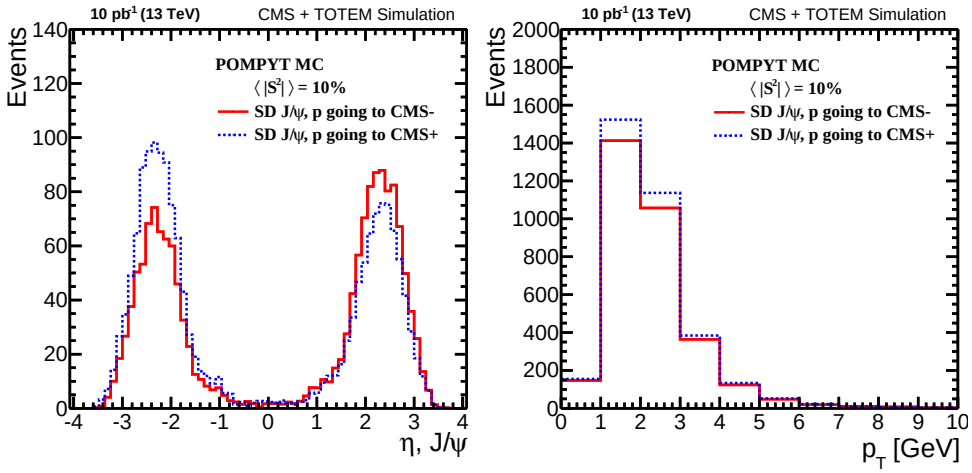

Figure 7: Distributions of the pseudorapidity of the $J/\psi(\mu^+\mu^-)$ system (left) and the transverse momentum of the leading muons (right) in $J/\psi(\mu^+\mu^-)$ events. Events with a proton detected in the CMS z-negative (positive) direction are shown in solid red (dashed blue) line. Events were simulated with the POMPYT MC and normalized to an integrated luminosity of 10 pb^{-1}. A gap survival probability of 10% was used.

4.3 Central exclusive dijet production

The infrared and collinear safe anti-k_T jet clustering algorithm with a size parameter $R = 0.5$ is used to reconstruct jets. The jet momentum is determined as the vectorial sum of all particle momenta inside it. The following criteria were used to select CEP dijet events:

- A proton was required to be within the acceptance of the RP stations simultaneously in both sides of the interaction point;
- A single reconstructed vertex was required. This cut rejects events with additional pileup interactions for which a primary vertex is reconstructed;
- The two leading jets (largest p_T) were required to have $p_T > 30$ GeV;
- Jets were selected in the CMS central detector acceptance, $|\eta| < 2.5$.

The fraction of selected events is 0.011. Selected events were weighted by the product $\mathcal{A}^+ \times \mathcal{A}^-$, where $\mathcal{A}^-$ ($\mathcal{A}^+$) is the acceptance of a proton tagged in the RP stations in the CMS z-negative (positive) direction, as shown in Figure 2. The product $\mathcal{A}^+ \times \mathcal{A}^-$ corresponds to the probability of finding a proton in the detectors in both sides of the interaction point. The average of the product $\mathcal{A}^+ \times \mathcal{A}^-$ is around 25%.

Figure 8 shows the event distribution of the fractional momentum loss ξ of the outgoing protons. As discussed in Section 3, events were simulated with a minimum invariant mass of the central system of $M_{jj}^{Gen} > 100$ GeV at the generator level. Figure 9 shows the distributions of the pseudorapidity, the transverse momentum p_T and the invariant mass M_{jj} of the leading and second-leading jets in CEP dijet events.

Figure 10 shows the event distributions of the fractions M_{jj}/M_{pf} and M_{jj}/M_X, where M_{pf} is the invariant mass of all reconstructed particles associated with the vertex of the dijet system, and M_X is the mass of the central system, calculated from the momentum loss of the outgoing protons, $M_X = \sqrt{s\xi_1\xi_2}$. CEP events populate the region of these variables towards ~ 1. They can be used to enhance a CEP signal contribution [37, 38].

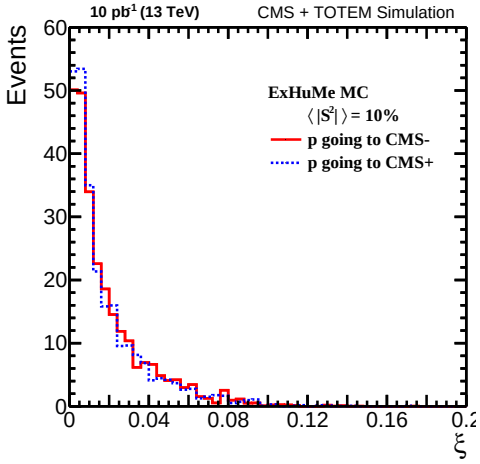

Figure 8: Distribution of the fractional momentum loss ξ of the outgoing protons in CEP dijet events. Outgoing protons in the CMS z-negative direction are shown in red (solid line) and protons in the CMS z-positive direction in blue (dashed line). Events were simulated with the ExHuME MC with a minimum invariant mass of the central system of $M_{jj}^{Gen} > 100$ GeV, and normalized to an integrated luminosity of 10 pb^{-1}. A gap survival probability of 10% was used.

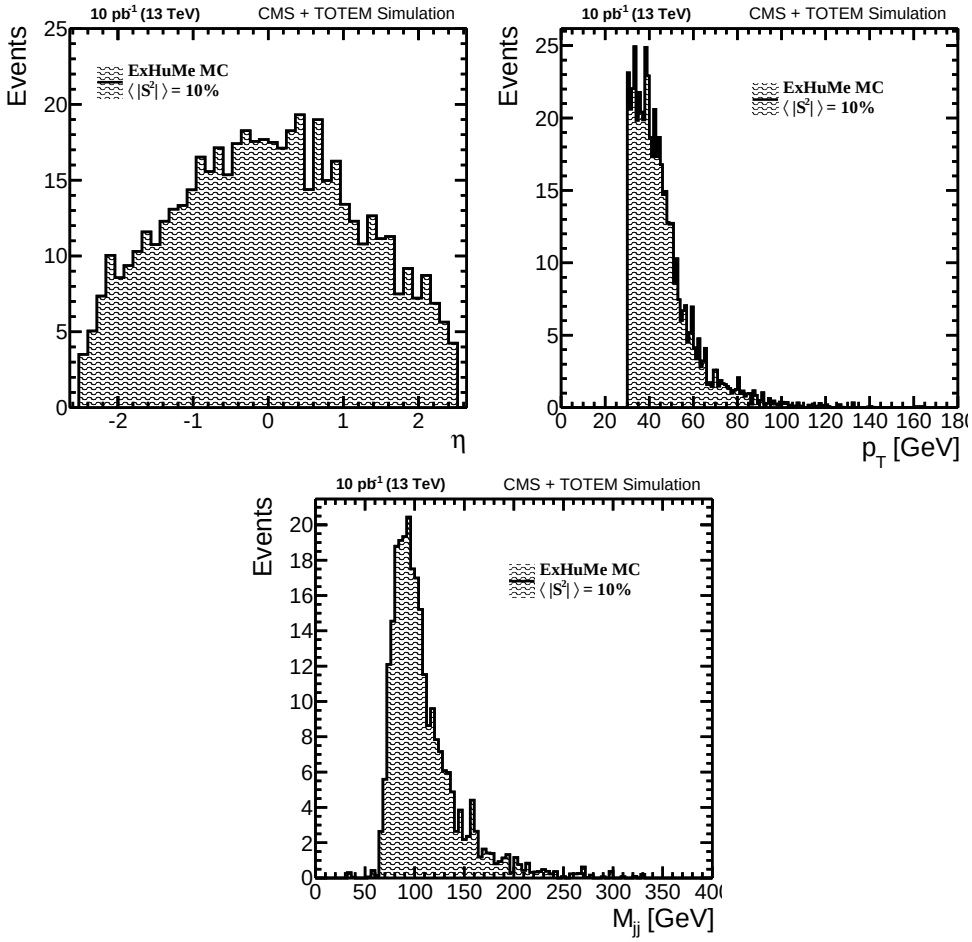

Figure 9: Distributions of the pseudorapidity (left), transverse momentum (right) and the invariant mass M_{jj} (bottom) of the leading and second-leading jets. Events were simulated with the ExHuME MC with a minimum invariant mass of the central system of $M_{jj}^{Gen} > 100$ GeV, and normalized to an integrated luminosity of 10 pb^{-1}. A gap survival probability of 10% was used.

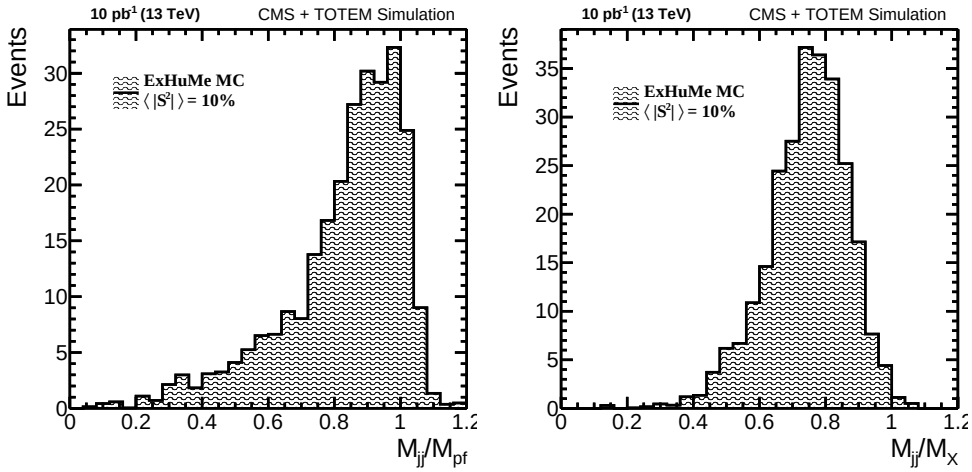

Figure 10: Event distributions of the fractions M_{jj}/M_{pf} (left) and M_{jj}/M_X (right). M_X using generator level information. Events were simulated with the EXHUME MC with a minimum invariant mass of the central system of $M_{jj}^{Gen} > 100$ GeV, and normalized to an integrated luminosity of 10 pb^{-1}. A gap survival probability of 10% was used.

In this analysis the Double Pomeron Exchange (DPE) dijet contribution, i.e. $pp \to pXp$ where X includes a dijet system, has not been included. It is an irreducible background when a dijet system is selected along with two outgoing protons. In a study assuming high-luminosity running and low-β^*, and in a higher-mass region [38], it has been shown that this background can be largely reduced when requiring the lack of charged particle activity not associated to the dijet system in the central detector, and by exploiting correlations between the dijet system and the properties of the outgoing protons such as the dijet mass ratio shown in Figure 10.

5 Visible cross section and event yields

The evaluation of the visible cross section (σ_{vis}) is derived in this section for SD Z or W boson, SD J/ψ and CEP dijet production. These numbers are used to roughly estimate the number of reconstructed events that can be detected using common runs with CMS and TOTEM. The different sources of physics and beam backgrounds, as well as the effect of the trigger selection and systematic uncertainties are not included in these results.

5.1 Trigger

In Run II the trigger strategy will be similar to the one in 2012: the electronic logic accept signal (L1-accept) from CMS (TOTEM) was sent to TOTEM (CMS) to trigger the readout of the detectors. In 2012, with 112 bunches and a pileup probability of ~ 0.07, the electronic detector trigger (L1) selections and corresponding rates were:

- for SD Z or W selection: at least one muon (electron) with $p_T > 7$ GeV (57 Hz) and another that required at least two muons (electrons) with $p_T > 3$ GeV (22 Hz);
- for SD J/ψ selection: at least two muons with any $p_T > 0$ GeV and $|\eta| < 2.45$ and no isolation or charge requirements (45 Hz);
- for CEP dijets: at least two jets with $p_T > 20$ GeV and $|\eta| < 5.0$ (75 Hz).

For processes like CEP dijet production, which require protons on both arms of RPs, a coincidence with a logical accept signal from both RP (L1-RP trigger) is foreseen to reduce the overall

trigger rate.

5.2 Background

Due to the detection of the leading proton with the RP, non-diffractive backgrounds can be largely suppressed. However, if they overlap with one or more pileup events with an outgoing proton which is detected in the RP stations, they can potentially be misidentified as a diffractive event. Additional particles moving along the LHC beam, or beam-halo, can also be detected in the RP stations and, when associated simultaneously with a non-diffractive event, act as a background.

These sources of background are not included in the results presented. In low-luminosity, low-pileup conditions as those considered for the LHC Run II scenarios shown in Section 1.1, they can however be largely suppressed when taking into account the correlations between the information observed with the CMS detector alone, and that from the outgoing protons measured at the RP stations.

In the method presented in Ref. [39] the difference between the longitudinal momentum loss of the proton reconstructed with CMS (ξ_{CMS}) and that reconstructed with the TOTEM RPs (ξ_{TOTEM}) is used to suppress the pileup and beam-halo backgrounds. Background events populate the kinematically forbidden region $\xi_{\mathrm{CMS}} - \xi_{\mathrm{TOTEM}} > 0$. The requirement $\xi_{\mathrm{CMS}} - \xi_{\mathrm{TOTEM}} < 0$ is shown to select mostly signal events. The remaining contamination of background was found to be $\sim 4\%$. The background estimate was obtained from a mixture of Monte Carlo including non-diffractive events and zero-bias (ZB) data events. The mixture MC+ZB was passed through the analysis selection procedure. The ZB data sample includes both events with protons originating from pileup and particles from beam-halo hitting the RP detectors. This study is based on the data collected with the CMS and TOTEM detectors in proton-proton collisions at $\sqrt{s} = 8$ TeV during a dedicated run with $\beta^* = 90$ m, in 2012, with similar conditions as those expected for the low-luminosity, low-pileup scenarios during the LHC Run II in 2015.

5.3 Results

Table 3 summarizes the results of the visible cross section (σ_{vis}) calculation for the electron and muon channels of SD Z or W boson production and SD $J/\psi(\mu^+\mu^-)$ production.

Table 3: Overview of the visible cross section values obtained in the SD $\mathrm{Z} \to \mathrm{e}^+\mathrm{e}^-$, $\mathrm{Z} \to \mu^+\mu^-$, $\mathrm{W} \to \mathrm{e}\nu_e$, $\mathrm{W} \to \mu\nu_\mu$ and $J/\psi \to \mu^+\mu^-$ production channels, shown for events with a proton detected in the CMS z-negative or z-positive directions. The uncertainties shown are statistical.

	$\mathrm{Z} \to \mathrm{e}^+\mathrm{e}^-$	$\mathrm{Z} \to \mu^+\mu^-$	$\mathrm{W}^+ \to \mathrm{e}^+\nu_e$ $\mathrm{W}^- \to \mathrm{e}^-\bar{\nu}_e$	$\mathrm{W}^+ \to \mu^+\nu_\mu$ $\mathrm{W}^- \to \mu^-\bar{\nu}_\mu$	$J/\psi(\mu^+\mu^-)$
σ_{vis} [pb]	1.34 ± 0.02	2.04 ± 0.02	16.37 ± 0.21	20.30 ± 0.23	332.5 ± 2.9

The total visible cross section, estimated by summing all Z channels, is 3.38 ± 0.03 pb whereas for the sum of all W channels it is 36.7 ± 0.3 pb. Finally, for $J/\psi(\mu^+\mu^-)$ the visible cross section is 332.5 ± 2.9 pb.

The visible cross section (σ_{vis}) obtained for CEP dijet production is 26.1 ± 3.6 pb; it corresponds to events with $\mathrm{M}_{\mathrm{jj}}^{\mathrm{Gen}} > 100$ GeV at the generator level.

In two weeks of pp data taking, and depending on the Run II LHC beam optics setup, single-diffractive Z or W boson and $J/\psi(\mu^+\mu^-)$ production and central exclusive dijet production

could be observed. Table 4 gives an overview of the expected event yields assuming an integrated luminosity of 10 pb^{-1}. The results shown in Table 4 are further corrected by the TOTEM RP proton reconstruction efficiency of $92.5 \pm 2.5\%$ [40].

Table 4: Overview of the expected event yields for an integrated luminosity of 10 pb^{-1} in the SD Z or W and J/ψ production channels, as well as for CEP dijet production, with $M_{jj}^{Gen} > 100$ GeV. The uncertainties shown are statistical.

LHC Scenario	SD Boson Z	SD Boson W	SD J/ψ	CEP dijet ($M_{jj}^{Gen} > 100$ GeV)
10 pb^{-1}	30 ± 1	340 ± 10	3080 ± 90	240 ± 34

6 Summary

Visible cross sections for single-diffractive Z and W boson production, single-diffractive J/ψ production, and CEP dijet production were estimated, assuming a high-β^* and low-pileup scenario during the LHC Run II. Events were selected using the CMS and TOTEM detectors, with Roman pot tagging to identify the outgoing protons from diffractive events. Monte Carlo simulations were used to describe the detector response. Possible trigger strategies have been presented.

The predictions presented rely on the Monte Carlo models, where the contribution from proton dissociation is not included. The visible cross section estimates and event yields are proportional to the rapidity gap survival probability of 10% used throughout this study.

The conditions expected for the low-luminosity, low-pileup scenarios during the LHC Run II in 2015, with proton-proton collisions at $\sqrt{s} = 13$ TeV, are similar to those obtained during a dedicated run with $\beta^* = 90$ m, in 2012, when CMS and TOTEM collected data simultaneously from proton-proton collisions at $\sqrt{s} = 8$ TeV, with an integrated luminosity of roughly 50 nb^{-1}. According to the expected event yields that has been presented, a minimum amount of 10 pb^{-1} of data with low-pileup is necessary to perform a measurement.

References

[1] J. Bjorken, "Rapidity gaps and jets as a new physics signature in very high-energy hadron hadron collisions", *Phys.Rev.* **D47** (1993) 101–113, doi:10.1103/PhysRevD.47.101.

[2] CDF Collaboration, "Diffraction Results from CDF", (2012). arXiv:1204.5241. Comments: 5 pages, 2 figures, Presented at XIX International Workshop on Deep-Inelastic Scattering and Related Subjects (DIS 2011).

[3] P. Collins, "An Introduction to Regge Theory and High-EnergyPhysics". Cambridge University Press, 1977.

[4] M. Arneodo and M. Diehl, "Diffraction for non-believers", (2005). arXiv:0511047. Comment: 23 pages, 26 figures. Contributed to the Proceedings of the Workshop on HERA and the LHC, DESY and CERN, 2004-2005.

[5] V. Gribov, "Possible Asymptotic Behavior of Elastic Scattering", *JETP Lett.* **41** (1961) 667–669.

[6] V. Khoze et al., "Diffractive processes as a tool for searching for new physics", (2005). arXiv:hep-ph/0507040. DCPT-05-72, IPPP-05-36.

[7] M. Albrow, T. Coughlin, and J. Forshaw, "Central Exclusive Particle Production at High Energy Hadron Colliders", *Prog. Part. Nucl. Phys.* **65** (2010) 149–184, doi:10.1016/j.ppnp.2010.06.001, arXiv:1006.1289.

[8] CMS Collaboration, "Study of single-diffractive production of W bosons at the LHC", CMS Physics Analysis Summary CMS-PAS-DIF-07-002, CERN, Geneva, 2009.

[9] TOTEM Collaboration, "TOTEM Upgrade Proposal", Technical Report CERN-LHCC-2013-009. LHCC-P-007, CERN, Geneva, 2013.

[10] TOTEM Collaboration, "Timing Measurements in the Vertical Roman Pots of the TOTEM Experiment", Technical Report CERN-LHCC-2014-020. TOTEM-TDR-002, CERN, Geneva, Sep, 2014.

[11] V. Andreev et al., "Performance studies of a full-length prototype for the CASTOR forward calorimeter at the CMS experiment", *Eur.Phys.J.* **C67** (2010) 601–615, doi:10.1140/epjc/s10052-010-1316-4.

[12] A. J. Bell et al., "Physics and Beam Monitoring with Forward Shower Counters (FSC) in CMS", (2012). FERMILAB-PUB-10-718-CMS, CMS-NOTE-2010-015, CERN-CMS-NOTE-2010-015.

[13] CMS Collaboration, "The CMS experiment at the CERN LHC", *JINST* **3** (2008) S08004, doi:10.1088/1748-0221/3/08/S08004.

[14] CMS Collaboration, "Particle-Flow Event Reconstruction in CMS and Performance for Jets, Taus, and MET", CMS Physics Analysis Summary CMS-PAS-PFT-09-001, CERN, Geneva, 2009.

[15] CMS Collaboration, "Commissioning of the Particle-flow Event Reconstruction with the first LHC collisions recorded in the CMS detector", CMS Physics Analysis Summary CMS-PAS-PFT-10-001, CERN, Geneva, 2010.

[16] M. Cacciari, G. P. Salam, and G. Soyez, "The Anti-k(t) jet clustering algorithm", *JHEP* **04** (2008) 063, doi:10.1088/1126-6708/2008/04/063, arXiv:0802.1189.

[17] CMS Collaboration, "Energy Calibration and Resolution of the CMS Electromagnetic Calorimeter in pp Collisions at $\sqrt{s} = 7$ TeV", *JINST* **8** (2013) P09009, doi:10.1088/1748-0221/8/09/P09009, arXiv:1306.2016.

[18] CMS Collaboration, "Determination of jet energy calibration and transverse momentum resolution in CMS", *Journal of Instrumentation* **6** (2011) 11002, doi:0.1088/1748-0221/6/11/P11002, arXiv:1107.4277.

[19] TOTEM Collaboration, "The TOTEM experiment at the CERN Large Hadron Collider", *JINST* **3** (2008) S08007, doi:10.1088/1748-0221/3/08/S08007.

[20] TOTEM Collaboration, "Performance of the Totem Detectors at the LHC", *Int. J. Mod. Phys. A* **A28** (2013) 1330046, doi:10.1142/S0217751X13300469, arXiv:1310.2908.

[21] GEANT4 Collaboration, "GEANT4: A simulation toolkit", *Nucl. Instrum. Meth.* **A506** (2003) 250–303, doi:10.1016/S0168-9002(03)01368-8.

[22] T. Sjöstrand, S. Mrenna, and P. Z. Skands, "A Brief Introduction to PYTHIA 8.1", *Comput.Phys.Commun.* **178** (2008) 852–867, doi:10.1016/j.cpc.2008.01.036, arXiv:0710.3820.

[23] B. E. Cox and J. R. Forshaw, "POMWIG: HERWIG for diffractive interactions", *Comput. Phys. Commun.* **144** (2002) 104–110, doi:10.1016/S0010-4655(01)00467-2, arXiv:hep-ph/0010303.

[24] P. Bruni and G. Ingelman, "Diffractive hard scattering at ep and p anti-p colliders", DESY REPORT DESY 93-187, CERN, 1993.

[25] J. Monk and A. Pilkington, "ExHuME: A Monte Carlo event generator for exclusive diffraction", *Comput. Phys. Commun.* **175** (2006) 232–239, doi:10.1016/j.cpc.2006.04.005, arXiv:hep-ph/0502077.

[26] G. Corcella et al., "HERWIG 6: An Event generator for hadron emission reactions with interfering gluons (including supersymmetric processes)", *JHEP* **01** (2001) 010, doi:10.1088/1126-6708/2001/01/010, arXiv:hep-ph/0011363.

[27] H1 Collaboration, "Measurement and QCD analysis of the diffractive deep-inelastic scattering cross-section at HERA", *Eur. Phys. J.* **C48** (2006) 715–748, doi:10.1140/epjc/s10052-006-0035-3, arXiv:hep-ex/0606004.

[28] J. Pumplin et al., "New generation of parton distributions with uncertainties from global QCD analysis", *JHEP* **07** (2002) 012, doi:10.1088/1126-6708/2002/07/012, arXiv:hep-ph/0201195.

[29] CMS Collaboration, "Observation of a diffractive contribution to dijet production in proton-proton collisions at $\sqrt{s} = 7$ TeV", *Phys. Rev.* **D87** (2013) 012006, doi:10.1103/PhysRevD.87.012006, arXiv:1209.1805.

[30] G. Ingelman and P. Schlein, "Jet structure in high mass diffractive scattering", *Physics Letters B* **152** (1985), no. 3, 256 – 260, doi:http://dx.doi.org/10.1016/0370-2693(85)91181-5.

[31] R. Field, "Physics at the Tevatron", in *XXXIV International Meeting on Fundamental Physics on April 27, 2006*. Acta Phys. Pol. B, 2008. (ACTA2008)039,2611.

[32] V. Khoze, A. Martin, and M. Ryskin, "Prospects for new physics observations in diffractive processes at the LHC and Tevatron", *The European Physical Journal C - Particles and Fields* **23** (2002), no. 2, 311–327, doi:10.1007/s100520100884.

[33] V. Khoze, A. Martin, and M. Ryskin, "Double-diffractive processes in high resolution missing-mass experiments at the Tevatron", *Eur. Phys. J.* **C19** (2001) 477–483, doi:10.1007/s100520100637.

[34] H. Niewiadomski, V. Avati, C. Da Via, and K. Eggert, "Reconstruction of Protons in the TOTEM Roman Pot Detectors at the LHC". PhD thesis, Manchester U., Manchester, 2008. Presented on 11 Sep 2008.

[35] CMS Collaboration, "Measurements of Inclusive W and Z Cross Sections in pp Collisions at $\sqrt{s} = 7$ TeV", *JHEP* **01** (2011) 080, doi:10.1007/JHEP01(2011)080, arXiv:1012.2466.

[36] CMS Collaboration, "Performance of CMS muon reconstruction in pp collision events at $\sqrt{s} = 7$ TeV", *JINST* **7** (2012) P10002, doi:10.1088/1748-0221/7/10/P10002, arXiv:1206.4071.

[37] CDF Collaboration, "Observation of Exclusive Dijet Production at the Fermilab Tevatron $p\bar{p}$ Collider", *Phys. Rev.* **D77** (2008) 052004, doi:10.1103/PhysRevD.77.052004, arXiv:0712.0604.

[38] CMS and TOTEM Collaborations, "CMS-TOTEM Precision Proton Spectrometer Technical Design Report", Tech. Design Report CMS-TDR-10, TOTEM-TDR-003, CERN-LHCC-2014-021, CERN, Geneva, 2014.

[39] CMS and TOTEM Collaborations, "Development of a beam-halo and pileup background rejection procedure for diffractive analyses in low-pileup runs based on Roman Pot tagging with the CMS and TOTEM experiments", CMS Detector Performance Summary, CERN, Geneva, 2014.

[40] TOTEM Collaboration, "Performance of the TOTEM Detectors at the LHC", *Int. J. Mod. Phys.* **A28** (2013) 1330046, doi:10.1142/S0217751X13300469, arXiv:1310.2908.